Analysis of High-Contrast All-Optical Dual Wavelength Switching in Asymmetric Dual-Core Fibers

Le Xuan The Tai[1], Mattia Longobucco[2,3,4], Nguyen Viet Hung[5], Bartosz Paluba[3], Marek Trippenbach[3] , Boris A. Malomed[6,7], Ignas Astrauskas[8], Audrius Pugzlys[8], Andrius Baltuska[8], Ryszard Buczynski[2,3], Ignac Bugar[8,9]

[1]*Faculty of Physics, Warsaw University of Technology, Koszykowa 75, 00-662 Warsaw, Poland.*
[2]*Department of Glass, Lukasiewicz Research Network Institute of*
Electronic Materials Technology, Wolczynska 133, 01-919 Warsaw, Poland.
[3]*Faculty of Physics, University of Warsaw, Pasteura 5, 02-093 Warsaw, Poland.*
[4]*School of Electrical and Electronics Engineering,*
Nanyang Technological University, 50 Nanyang Avenue, 639798 Singapore.
[5]*International Training Institute for Materials Science (ITIMS),*
Hanoi University of Science and Technology (HUST), No 1 - Dai Co Viet Str., Hanoi,Vietnam.
[6]*Department of Physical Electronics, School of Electrical Engineering, Faculty of Engineering,*
and Center for Light-Matter Interaction, Tel Aviv University, Tel Aviv 69978, Israel.
[7]*Instituto de Alta Investigacion, Universidad de Tarapaca, Casilla 7D, Arica, Chile.*
[8]*Photonics Institute, Vienna University of Technology, Gußhausstraße 25-29, Vienna, 1040, Austria.*
[9]*Institute of Chemistry and Environmental Sciences,*
University of Ss. Cyril and Methodius in Trnava, Nam. J. Herdu 2, 917 00 Trnava, Slovakia.

We systematically present experimental and theoretical results for the dual-wavelength switching of 1560 nm, 75 fs signal pulses (SPs) driven by 1030 nm, 270 fs control pulses (CPs) in a dual-core fiber (DCF). We demonstrate a switching contrast of 31.9 dB, corresponding to a propagation distance of 14 mm, achieved by launching temporally synchronized SP-CP pairs into the fast core of the DCF with moderate inter-core asymmetry. Our analysis employs a system of three coupled propagation equations to identify the compensation of the asymmetry by nonlinearity as the physical mechanism behind the efficient switching performance.

The realization of an all-optical switching in a simple fiber format has been a long-standing challenge in the field of nonlinear fiber optics [1–5]. The development of nonlinear directional couplers for all-optical switching holds great potential for many applications that require compact high-speed signal processing, without the use of free-space optics. Ultrafast nonlinear switching was proposed for femtosecond pulses in the normal-dispersion range of a step-index silica fiber coupler [6]. The main limitations of this approach are a relatively high power and the intra-channel and inter-modal dispersion phenomena, which strongly affect pulses with widths ~ 100 fs. Various other devices have been developed, including metamaterial-based switches [7], ring resonators [8], plasmonic waveguides [9], and nonlinear optical loop mirrors [10]. Nevertheless, when it comes to the fabrication simplicity and cascading, dual-core optical fibers (DCFs) remain the most attractive option [11–14]. In particular, a promising method of beam-by-beam cleaning, using orthogonally polarized fiber pulses, has been introduced recently [15] applicable also for all-optical switching tasks. Our motivation for studying nonlinear DCFs is stimulated by their potential for the reduction of the devices' length to the scale of centimeters or millimeters, in contrast to the aforementioned setups which require meter-scale fiber lengths [10, 15].

In the experimental study [14], we had produced the first evidence of dual-wavelength switching based on the interaction between two temporarily synchronized pulses using an all-solid DCF. The operation mode used a pair of femtosecond pulses simultaneously launched into the same fiber core. A longer-wavelength (1560 nm) low-energy pulse served as a signal pulse (SP), and the shorter-wavelength one (1030 nm) with higher energy was a control pulse (CP). Using the synchronized pair of pulses with the appropriate CP energy, SP switching between the excited and originally idle cores was demonstrated, with negligible distortion. This scenario is more efficient than the earlier reported straightforward energy control of a single ultrashort pulse (*self-switching*) [16–20], as it balances the inter-core asymmetry. The asymmetry is inherent to DCFs, being a basic limiting factor of the high-contrast directional-coupler performance. Accordingly, the two cores of an asymmetric DCF are identified as fast and slow ones, with effective refractive indices $n_{\mathrm{f}} < n_{\mathrm{s}}$. The motivation for the use of the nonlinear dual-wavelength interaction is that, in the time window defined by its duration, the co-propagating CP reduces the group velocity of the fast core to the level of the slow one, if the pulse pair is launched into the fast core [14]. An important aspect of this approach is the strong spectral dependence of the coupling length, which prevents the energy transfer of the shorter-wavelength CP pulses to the idle core. As a result, the switching contrasts > 25 dB was recorded, exceeding the best experimental results for the self-switching in the C-band [18] and the theoretical prediction for the ultrafast soliton self-trapping in highly nonlinear DCFs [16]. Additionally, shorter 14 mm fibers were used, instead of the 35 mm one used in the study of self-switching at the signal wavelength of 1550 nm.

However, the dual-wavelength switching scheme has its

drawbacks – mainly, relatively high CP energies, $\sim$ a few nJ. Here we present an advanced experimental study, also supported by numerical simulations, in which the fiber length, CP energy, and the CP-SP delay were simultaneously optimized, thus leading to the reduction of the switching energy to the sub-nJ range, while preserving the high switching-contrast level.

In this work, we used simple-cladding all-solid DCFs with the cross-section displayed in Fig. 1 (left), similar to the samples used in previous works [14, 18], which provide more details. The distance between the core centers is 3.1 μm, and the effective mode area of both cores is ≈ 1.41 μm^2. The fiber is made of two thermally matched soft glasses (lead-silicate and borosilicate for the cores and cladding, respectively), with a very high refractive-index contrast $\simeq 0.4$ between the core and cladding in the C-band. The nonlinear refractive index in the core lead-silicate glass is 20 times higher than in the silica glass [21]. The mismatch between the fast and slow cores is $\delta n_\mathrm{a} = n_\mathrm{s} - n_\mathrm{f} = 1.214 \cdot 10^{-4}$. The experimental setup includes two laser arms generating femtosecond CPs (1030 nm, 270 fs ones produced by a commercial ultrafast Yb:KGW amplifier - Pharos, Light Conversion) and SPs (1560 nm, 75 fs ones from a self-made double-pass optical parametric amplifier pumped by the second harmonic of the same Yb:KGW amplifier), at the repetition rate of 10 kHz. The two pulses were combined by a dichroic mirror and synchronized by a delay line placed in the control arm. The CP energy and polarization were managed independently, using two half-wave plates and by a Glan-Taylor polarizer placed between them. After passing the fiber, the control field was selectively filtered out a by a high-reflectance mirror, securing that only the signal field from the DCF output facet was imaged on a multimode collection fiber of a spectrometer or infrared (IR) camera.

Similar to the findings in Ref. [14], a series of CP spatial and spectral distributions of the CP output field were separately recorded from both cores. In addition to investigating the effects of fiber length, and the choice of the excited core (fast or slow), our study extends its focus to examine the CP-SP delay effect. The camera images were processed by calculating the dual-core extinction ratio (ER), separately integrating the intensity distribution in the area of each core. Fig. 1 (right) shows the camera images at the output facet of the DCF with an optimal length of 14 mm, following the excitation of the fast and slow cores (top and bottom series, respectively). The results reveal that the excitation of the fast core provides efficient switching performance, thanks to the above-mentioned DC asymmetry-balancing principle [14]. The switching contrast (maximal ΔER) is 31.9 dB between control-energy levels 0.2 and 0.6 nJ, at which the highest and lowest ERs were recorded, respectively. In the case of the slow core excitation (the bottom series in Fig. 1), no switching performance was observed. Therefore, we report results solely for the fast-core excitation.

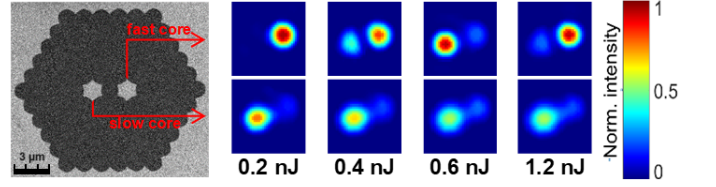The DCF is modelled by coupled nonlinear Schrödinger

FIG. 1. Left: The scanning-electron-microscope image of the cross-section of the all-solid DCF. Top and bottom series: IR-camera images of the 1560 nm, 75 fs SP field at the DCF output depending on energy of the 1030 nm, 270 fs CP exciting the fast and slow cores, respectively, of a 14 mm length DCF.

equations (NLSEs). For CP amplitude A_0, which propagates only in the excited core, NLSE is

$$\partial_z A_0 = -\beta_{10}\partial_t A_0 - (i/2)\beta_{20}\partial_t^2 A_0 + i\gamma|A_0|^2 A_0, \quad (1)$$

where z and t are the propagation distance and time in physical units, and coefficients β_{10}, and β_{20}, γ, represent the inverse group velocity, group-velocity dispersion (GVD), and SPM nonlinearity, respectively. NLSEs for the SP amplitudes in the excited and idle cores (in the simulation framework are always the fast and slow, respectively) are

$$\partial_z A_f = -\beta_{1f}\partial_t A_f - (i/2)\beta_{2f}\partial_t^2 A_f +$$
$$i\kappa_0 A_s - \kappa_1\partial_t A_s - 2i\delta A_f + i\gamma|A_0|^2 A_f,$$
$$\partial_z A_s = -\beta_{1s}\partial_t A_s - (i/2)\beta_{2s}\partial_t^2 A_s +$$
$$i\kappa_0 A_f - \kappa_1\partial_t A_f, \quad (2)$$

where $\beta_{1f} = \beta_{1s} \equiv \beta_1 \neq \beta_{10}$ is the SP inverse group velocity, $\beta_{2f} = \beta_{2s} = \beta_2$ is the SP GVD, γ is the XPM coefficient, $\delta = (\beta_{0f} - \beta_{0s})/2$ is the inter-core propagation constant difference, κ_0 and κ_1 being zeroth- and first-order coupling coefficients.

By means of rescaling and introducing retarded time $\tau = \sqrt{\kappa_0/|\beta_2|}t - \beta_{10}z$, and rescaling $\zeta = \kappa_0 z$, $\psi = \sqrt{\gamma/\kappa_0}A_0$ and $\phi_{f,s} = \sqrt{\gamma/\kappa_0}A_{f,s}$, Eqs. (1) and (2) are cast in the normalized form, with $\beta_2 = \gamma = \kappa \equiv 1$. In particular, the rescaled equation for CP is

$$i\partial_\zeta \psi = \frac{\beta_{20}}{2\beta_2}\partial_\tau^2 \psi - |\psi|^2\psi. \quad (3)$$

The CP input in the fast core, with amplitude a_{CP} and FWHM temporal size T_{CP} is $\psi(z = 0, \tau) = a_{CP}\exp[-(\tau/w_{CP})^2]$, where $w_{CP} = T_{CP}/\left(1.1774\sqrt{|\beta_2|/\kappa_0}\right)$. The set of the rescaled equations contains three adjustable parameters: the inverse-group-velocity CP-SP mismatch $\alpha = (\beta_1 - \beta_{10})/\sqrt{|\beta|/\kappa_0}$, the inter-core index mismatch $\sigma = \delta/\kappa_0$, and the dispersive coupling coefficient $\epsilon = \kappa_1/\sqrt{\kappa_0|\beta_2|}$.

The SP input with amplitude a_{SP} and FWHM size T_{SP} in the fast channel is $\phi_f(0, \tau) = a_{SP}\exp\{-[(\tau -$

$d)/w_{SP}]^2\}$, where $w_{SP} = T_{SP}/\left(1.1774\sqrt{|\beta_2|/\kappa_0}\right)$ and d is the CP-SP delay. The units of the propagation length and time in the experiment are $t_0 \equiv \sqrt{|\beta_2|/\kappa_0} = 24.9854$ fs and $z_0 \equiv 1/\kappa_0 = 8.11402$ mm. The corresponding CP energy is

$$E = \int_{-\infty}^{+\infty} |A_0(0,\tau)|^2 t_0 d\tau = \kappa_0 \tau_0 a_{CP}^2 w_{CP} \gamma^{-1}$$
$$\approx 15.189 a_{CP}^2 \text{ pJ}. \qquad (4)$$

The CP and SP widths are $T_{CP} = 270$ fs and $T_{SP} = 75$ fs. The effective coupling is $\kappa_{\text{eff}} \equiv \sqrt{\kappa_0^2 + \delta^2} = 0.90098$ mm^{-1}, where $\kappa_0 = 0.12324$ mm^{-1}. In the scaled units, the widths are $w_{CP} = 9.1780$, $w_{SP} = 2.5494$.

We simulated the pulse propagation in the parameter range corresponding to the experiment performed with the 14 mm long fiber and nonlinearity coefficient $\gamma = 1.86\,(\text{W·m})^{-1}$. Parameter values for the simulations were produced by Lumerical at the CP and SP wavelengths $\lambda = 1030$ nm and 1560 nm, respectively. While CP is affected by GVD and SPM, for the relatively weak SP, the only essential nonlinear effect is the XPM interaction with CP in the fast core. Results of the simulations are presented in Fig. 2. Panel a) reports cross-transfer of the SP in the symmetric DCF in the course of half a period of the inter-core oscillations. In the asymmetric DCF, where the oscillation period decreases due to mismatch, the transfer is dramatically reduced, as shown by the continuous wavy lines in panel b). The CP with appropriate energy compensates the mismatch in the asymmetric DCF, as shown by the dotted lines in the same panel. If the CP energy is not optimized, the switching performance may still be poor, as shown by the dashed lines. The optimization has to be performed by adjusting the CP-SP delay, fiber length, and CP energy. Panel c) shows that the optimization is also possible for longer DCFs. In this case, more oscillations are observed in the absence of CP, and effective switching is achieved with an appropriate CP energy. In the last panel of Fig. 2, we display the CP and SP shapes and their relative walkoff, when they propagate together along the fiber, for the parameters corresponding to our experiment.

In the absence of the CP, SPM, and higher-order coupling, the coupled equations admits an exact solution, which includes both the mismatch and dispersion. It is given by a two-component chirped Gaussian pulse moving along the temporal coordinate, with the components periodically oscillating between the cores:

$$\phi_1 = \Phi(\zeta)\left[i\sigma\sin\left(\sqrt{1+\sigma^2}\zeta\right) + \sqrt{1+\sigma^2}\cos\left(\sqrt{1+\sigma^2}\zeta\right)\right],$$
$$\phi_2 = -i\Phi(\zeta)\sin\left(\sqrt{1+\sigma^2}\zeta\right), \qquad (5)$$

where $\Phi(\zeta) = \frac{W}{\sqrt{W^2+i\zeta}}\exp[-\frac{(T+\Omega\zeta)^2}{2(W^2+i\zeta)} - i\Omega T - \frac{i}{2}\Omega^2\zeta]$. This solution depends on two arbitrary parameters,

width W and frequency shift Ω. The oscillation period is clearly mismatch ($\sigma-$) dependent, cf. Fig. 2.
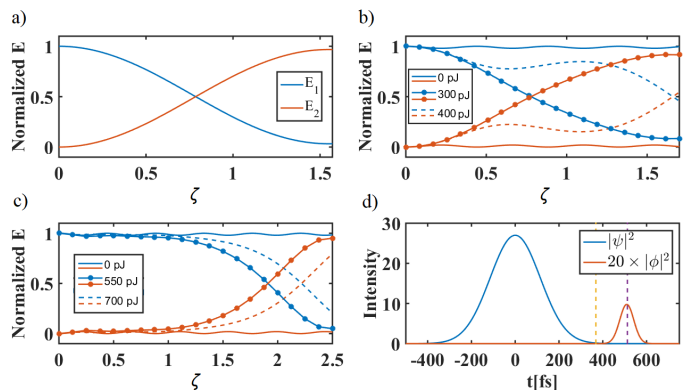

FIG. 2. Simulated switching performance in the DCF: a) Symmetric coupler: perfect cross-transfer of the SP. b) Asymmetric coupler: oscillations with negligible transfer in the absence of CP (continuous lines), the best performance provided by CP energy of 300 pJ (dotted lines). Dashed lines illustrate the situation when the CP energy is too high (400pJ). c) Compensation of the SP mismatch by the CP of 550 pJ energy for longer DCFs. d) CP and SP shapes. The distance between vertical dashed lines displays their relative walk-off over the DCF length.

To further characterize the switching performance, we address the dependence of the output extinction ratio, $\text{ER} = 10\log(E_f/E_s)$, on the CP-SP delay and CP power. The theoretical and experimental dependences on the delay are reported in Fig. 3a), showing that the ER is minimized at larger values of the delay with increasing the CP energy, in agreement with the above-mentioned asymmetry-compensation principle. Indeed, at higher energies, the SP experiences the same refractive-index change at a larger delay in the CP tail. The simulations predict a minimum of ER at the level of -10 dB at the energies in the range of $280-300$ pJ and around the delay of 75 fs. Taking into regard the 150 fs walkoff produced by the 14 mm long DCF [14], such conditions imply the SP moving in the peak area of the CP. Experimental results do not reveal so low ER because of additional CP nonlinear distortions (not included in the model), that may be significant around the CP peak. On the other hand, the predicted delay dependence at 320 pJ resembles the experimental curve (the inset in Fig. 3a) both in terms of the ER minimum level and delay range where ER is negative. Note that the experimental curve was obtained for 490 pJ CP energy, which also indicates that distortions affect the CP, impeding to reach the compensation effect at higher energies. In Fig. 3b) we plot the ER dependence on the CP energy for the CP-SP delay in the range of $125-175$ fs. These curves confirm that the ER minima are experimentally accessible with the 150 fs delay, which is an essential result, as the absolute delay was not identified in the experiment. Furthermore, getting the best experimental result at the large delay suggests a possibility of improving our approach by sup-

pressing the walkoff. It is evident that, at zero walkoff, the two pulses should be launched without delay. This condition would allow the use of significantly lower CP energies, helping to mitigate the nonlinear distortions. A general inference is that there is a wide range of both CP-SP delays and CP energies where the high-contrast (low-ER) switching occurs in the robust form, i.e., when slight changes of these parameters do not compromise it.
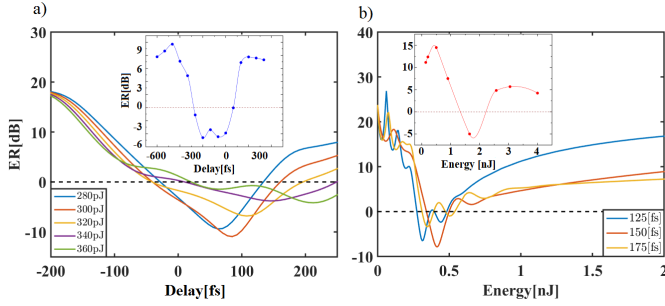

FIG. 3. Simulated ER dependence in the 14 mm long DCF on: a) the CP-SP delay for different CP energies; b) the CP energy for different delays. Insets present the experimental results for the CP energy 490 pJ in a), and for delay of 167 fs in b).

Finally, we have performed simulations varying the delay for $\sigma = 7.033$, $\alpha = -3.5$, $E_{CP} = 320$ pJ, at 14 mm DCF length, and analyzed the spectral shape of the output SPs. The results are reported in Fig. 4b, where the experimental spectra are in panel a). The numerical results, which are in qualitative agreement with the experimental counterparts, produce, for positive delays, a red-shifted and slightly broader SP spectrum. In the case of the negative delay, also the predicted blue shift and spectral narrowing were observed. It is worth mentioning that the solid lines are nearly identical in the case of experimental spectra and were registered at delays -533.6 fs and 800.4 fs from the excited core. Thus, they represent situations without overlap between CP-SP pulses and can be considered as original SP spectra.

Thus, we have conducted a detailed analysis of the dual-wavelength switching of 1560 nm, 75 fs SPs in the DCF, using the interaction with 1030 nm, 270 fs CPs as a nonlinear drive. Effects of the fiber length, CP energy, and CP-SP time delay on the switching performance have been studied, experimentally and numerically. The highest switching contrast of 31.9 dB was achieved in the 14 mm long DCF, with a broadband character in the spectral range of $1450 - 1650$ nm. The simulations reveal the role of the inter-core difference in the effective refractive index and CP-SP walk-off, confirming that the efficient switching is provided by the nonlinear balance of the inter-core asymmetry. Furthermore, the simultaneous effect of the CP energy and CP-SP delay on the dual-core ER was identified. One of the key advantages of our approach is the moderate nonlinear CP-SP interaction, which only slightly deforms the signal field. The
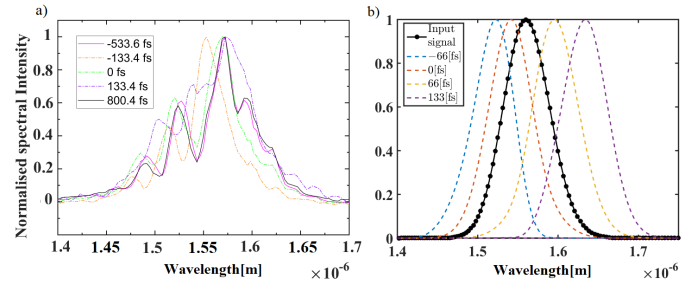

FIG. 4. Normalized SP spectra for different CP-SP delays at the output of the originally excited and idle cores (solid and dashed lines, respectively) at 14 mm DCF length. a) Experimental results at the CP energy of 600 pJ. b) Simulations for the CP energy of 320 pJ. Other parameters are $\alpha = -3.5$, $\epsilon = 0.3$ and $\sigma = 7.033$ corresponding to experimental values $\beta_1 - \beta_{10} = -111$ ps/m, $\kappa_1 = -0.921$ ps/m, $\delta = 865$ m^{-1}.

numerical results support this concept, producing moderate changes in the SP spectra. On the other hand, the experiment indicates more complex nonlinear distortions of CPs than predicted by the model and roughly its two times higher energy level. The reason of this discrepancy is that the presented model does not take into account the linear and nonlinear dissipative effects [20] in order to preserve the numerical stability of the rather complex three wave interaction in two coupled channels. Nevertheless, in the region of moderate nonlinear interaction - namely, when the SP overlaps with a CP's tail (delays exceeding 150 fs, Fig. 3) - the agreement between the experimental and numerical results is convincing.

To summarize, our study provides a comprehensive analysis of the dual-wavelength switching in the appropriately designed DCF. Our experimental and theoretical findings shed light on the physical mechanisms behind the observed phenomenology and highlight the advantages of the proposed approach, which makes it possible to achieve efficient switching while avoiding conspicuous distortion of the signal field. In the framework of the reported experiments, better matching of the SP and CP beams was ensured resulting in equal beam diameters at the DCF input. As a result, the energies at which the switching takes place are $\simeq 10$ times lower than those reported previously [14]. The sub-nJ, high-switching-contrast findings presented in this paper offer the application to the design of an all-optical signal-processing scheme. It may support a processing rate above 2 THz/s, primarily limited by the duration of the CP. By eliminating the walkoff, CP pulse durations below 100 fs can be applied, supporting processing rates up to 10 THz/s. Therefore, our approach offers significant advancements, primarily for the time-division-multiplexing tasks. However, the application to the wavelength-division multiplexing is limited by the femtosecond pulse duration and nonlinear interactions, resulting in pulse bandwidths ~ 100 nm. The theory presented here predicts the possibility of

further improvements in the switching contrast, while simultaneously reducing the CP energy, by suppressing the walkoff between the control and signal pulses. However, achieving such improvements will necessitate a meticulous engineering of the DCF design, optimizing both its dispersion and coupling characteristics. The development of such a new generation of DCFs may offer new applications to ultrafast signal processing and time-resolved spectroscopy.

Disclosures The authors declare no conflicts of interest.

Data Availability Data underlying the results presented in this paper are not publicly available at this time but may be obtained from the authors upon reasonable request.

[1] S. Wabnitz and B. J. Eggleton, All-Optical Signal Processing (Springer Series in Optical Sciences, 2015).

[2] J. Li, B.-E. Olsson, M. Karlsson, and P. Andrekson, J. Light. Technol. **23**, 2654 (2005).

[3] K. Kieu, L. Schneebeli, E. Merzlyak, J. M. Hales, A. DeSimone, J. W. Perry, R. A. Norwood, and N. Peyghambarian, Opt. Lett. **37**, 942 (2012).

[4] Q. Li, J. Song, X. Chen, M. Bi, M. Hu, and S. Li, Appl. Opt. **55**, 6880 (2016).

[5] S. M. Jensen, IEEE J. Quantum Electron. **18**, 1580 (1982).

[6] S. R. Friberg, A. M. Weiner, Y. Silberberg, B. G. Sfez, and P. S. Smith, Opt. Lett. **13**, 904 (1988).

[7] M. Papaioannou, E. Plum, J. Valente, E. T. F. Rogers, and N. I. Zheludev, APL Photonics **1**, 090801 (2016).

[8] S.-P. Su, C.-L. Wu, C.-H. Cheng, B.-J. Huang, H.-Y. Wang, C.-T. Tsai, Y.-H. Lin, Y.-C. Chi, M.-H. Shih, C.-K. Lee, and G.-R. Lin, ACS Photonics **3**, 806 (2016).

[9] M. Ono, M. Hata, M. Tsunekawa, K. Nozaki, H. Sumikura, H. Chiba, and M. Notomi, Nat. Photonics **14**, 37 (2020).

[10] T. Hirooka, R. Hirata, J. Wang, M. Yoshida, and M. Nakazawa, Opt. Express **26**, 27221 (2018).

[11] S. Trillo, S. Wabnitz, E. M. Wright, and G. I. Stegeman, Opt. Lett. **13**, 672 (1988).

[12] S. Minardi, F. Eilenberger, Y. V. Kartashov, A. Szameit, U. Ropke, J. Kobelke, K. Schuster, H. Bartelt, S. Nolte, L. Tomer, J. Lederer, A. Tiinnermann, and T. Pertsch, Phys. Rev. Lett. **105**, 263901 (2010).

[13] A. K. Sarma, Jpn. J. Appl. Phys. **47**, 5493 (2008).

[14] M. Longobucco, I. Astrauskas, A. Pugzlys, D. Pysz, F. Uherek, A. Baltuska, R. Buczynski, and I. Bugar, J. Light. Technol. **39**, 5111 (2021).

[15] M. Ferraro, F. Mangini, Y. Leventoux, A. Tonello, M. Zitelli, T. Mansuryan, Y. Sun, S. Fevrier, K. Krupa, D. Kharenko, S. Wabnitz, and V. Couderc, J. Light. Technol. **41**, 3164 (2023).

[16] M. Longobucco, J. Cimek, L. Curilla, D. Pysz, R. Buczynski, and I. Bugar, Opt. Fiber Technol. **51**, 48 (2019).

[17] M. Longobucco, J. Cimek, D. Pysz, R. Buczynski, and I. Bugar, Opt. Fiber Technol. **63**, 102514 (2021).

[18] M. Longobucco, I. Astrauskas, A. Pugzlys, N. T. Dang, D. Pysz, F. Uherek, A. Baltuska, R. Buczynski, and I. Bugar, Appl. Opt.**60**, 10191 (2021).

[19] V. H. Nguyen, L. X. T. Tai, I. Bugar, M. Longobucco, R. Buczynski, B. A. Malomed, and M. Trippenbach, Opt. Lett. **45**, 5221 (2020).

[20] V. H. Nguyen, L. X. T. Tai, M. Longobucco, R. Buczynski, I. Bugar, I. Astrauskas, A. Pugzlys, A. Baltuska, and M. T. Boris Malomed, Chaos, Solitons Fractals **167**, 113045 (2023).

[21] J. Cimek, N. Liaros, S. Couris, R. Stepien, M. Klimczak, and R. Buczynski, Opt. Mater. Express **7**, 3471 (2017).